Research Article | Vol. 11, No. 3 / 1 March 2020 / Biomedical Optics Express 1327
Biomedical Optics EXPRESS

Dual-mode line-field confocal optical coherence tomography for ultrahigh-resolution vertical and horizontal section imaging of human skin *in vivo*

JONAS OGIEN,[1,*] OLIVIER LEVECQ,[1] HICHAM AZIMANI,[1] AND ARNAUD DUBOIS[1,2]

[1] *DAMAE Medical, 28 rue de Turbigo, 75003 Paris, France*
[2] *Université Paris-Saclay, Institut d'Optique Graduate School, CNRS, Laboratoire Charles Fabry, 91127 Palaiseau, France*
[*] *jonas.ogien@damaemedical.fr*

Abstract: Line-field confocal optical coherence tomography (LC-OCT) is a recently introduced technique for ultrahigh-resolution vertical section (B-scan) imaging of human skin *in vivo*. This work presents a new implementation of the LC-OCT technique to obtain horizontal section images (C-scans) in addition to B-scans. C-scan imaging is achieved with this dual-mode LC-OCT system using a mirror galvanometer for lateral scanning along with a piezoelectric chip for modulation of the interferometric signal. A quasi-identical spatial resolution of ~ 1 µm is measured for both B-scans and C-scans. The images are acquired in both modes at a rate of 10 frames per second. The horizontal field of view of the C-scans is 1.2×0.5 mm^2, identical to the vertical field of view of the B-scans. The user can switch between the two modes by clicking a button. *In vivo* cellular-resolution imaging of human skin is demonstrated in both B-scan and C-scan modes, with the possibility to navigate within the skin tissues in real time.

1. Introduction

Line-field confocal optical coherence tomography (LC-OCT) is a recent imaging technique [1] based on the principle of time-domain OCT (TD-OCT) [2,3] with line illumination and line detection, that has been developed for acquiring vertical section images (B-scans) of skin tissues, *in vivo*, at ultrahigh resolution [4]. A single vertical scan is needed for the acquisition of a B-scan, during which focus tracking is performed, allowing the use of a high numerical aperture (NA) microscope objective to image with high lateral resolution. By using a supercontinuum laser as a light source and balancing the chromatic dispersion in the interferometer arms, the axial resolution of the LC-OCT images reaches the best axial resolution (~ 1 µm) achieved in OCT at comparable central wavelengths (~ 800 nm) [5,6]. Furthermore, the combination of line illumination and detection and of a high-NA objective provides an efficient confocal gate that improves the signal-to-noise ratio (SNR) by rejecting out-of-focus backscattered photons, although line confocal filtering is not as efficient as point confocal filtering [7]. A depth down to 500 µm is accessible within highly scattering samples such as human skin using LC-OCT [4].

Line illumination of the sample to avoid lateral scanning of a light beam has also been implemented in frequency-domain OCT (FD-OCT) [8–13]. Compared to LC-OCT, line-field FD-OCT has a significant advantage in image acquisition speed (about 100 times faster considering the same number of pixels per B-scan) [13]. However, line-field FD-OCT suffers from a limitation in lateral resolution since the focus cannot be adjusted during the acquisition of the information in depth, as it is acquired in parallel. The lateral resolution in line-field FD-OCT is limited to a few micrometers [14], while a lateral resolution of ~ 1 µm was demonstrated in LC-OCT [1].

Although LC-OCT has so far been used only for B-scan imaging, this technique has the potential to also produce en face (horizontal) section images (also referred to as C-scans), as

#385303 https://doi.org/10.1364/BOE.385303
Journal © 2020 Received 6 Dec 2019; revised 24 Jan 2020; accepted 27 Jan 2020; published 10 Feb 2020

Biomedical Optics EXPRESS

in optical coherence microscopy (OCM) [15,16], and more specifically in line-scanning OCM [7,17]. Developing an OCT system that can directly produce both B-scans and C-scans is interesting when true three-dimensional (volumetric) imaging is not desired, considering that C-scans are obtained in conventional OCT by reslicing a three-dimensional data-set acquired from a concatenation of adjacents B-scans.

In the field of dermatology, the predominant technique for obtaining in-depth en face images (C-scans) *in vivo* at high resolution is reflectance confocal microscopy (RCM). However, RCM does not provide high-resolution vertical section images (B-scans). Therefore, a system yielding both B-scans and C-scans with an isotropic spatial resolution comparable to the lateral resolution of RCM ($\sim$ 1 µm) would be particularly interesting. A common approach to obtain such high-resolution images is to reconstruct B-scan or C-scans from three-dimensional data obtained using OCM systems [18–21], nevertheless, this approach does not enable the real-time acquisition of images in both en face and vertical modes. Recently, a method was proposed for combining OCT and RCM, yielding OCT B-scans and RCM C-scans for skin imaging [22]. Nevertheless, even though the system was miniaturized enough to be integrated within a handheld probe [23], the combination of two distinct imaging techniques is fairly complex. Furthermore, the B-scans have a low lateral resolution ($\sim$ 10 µm), and the fact that the B-scans and C-scans have different resolution and contrast makes them difficult to correlate. Similarly, a system combining OCT for B-scan imaging and OCM for C-scan imaging was developed [24], but it also suffers from a resolution discrepancy between B-scans and C-scans. Furthermore the microscope objective has to be manually changed to switch from OCT to OCM imaging.

The purpose of this paper is to introduce an OCT technique capable of producing both B-scans and C-scans in real time with an ultrahigh isotropic resolution adapted for *in vivo* skin imaging. This system is based on an LC-OCT setup that has been modified to produce C-scans in addition to B-scans.

2. Methods

The approach proposed for acquiring C-scans using LC-OCT consists in scanning laterally on the sample the illumination line as achieved in line-scanning OCM [7,17], while B-scan acquisition is performed as in the initial LC-OCT system [4,25]. This strategy decouples the acquisition of B-scans and C-scans, resulting in two acquisition modes with independent speed limitations, making it possible to yield B-scans and C-scans in real time.

The LC-OCT setup for combined B-scan and C-scan imaging is presented in Fig. 1. It is based on a Linnik-type interferometer with a one-directional axial (depth) scanning device (piezoelectric stage, Physik Instrument, P625.1CD) for B-scan imaging and a one-directional lateral scanning device (mirror galvanometer, Cambridge Technology, 6220H) for C-scan imaging. It should be noted that the use of a mirror galvanometer allows C-scan images to be obtained from *in vivo* samples, which was not demonstrated in the previously reported line-scanning OCM system [17], where the sample had to be translated for C-scan imaging. A supercontinuum light source is used in conjunction with a collimator and a cylindrical lens to generate the illumination line, focused on the sample and imaged on a line-scan camera. All the components used for illumination and imaging (laser, optics, camera) are the same as those of the previously reported LC-OCT system [1,4]. The microscope objectives (20×, 0.5 NA) are also unchanged. Silicone oil is used as an immersion medium as its refractive index matches the one of skin (n $\sim$ 1.4). Glass plates are placed in both arms of the interferometer, for subject stabilization (in the sample arm) and for providing a $\sim$ 3.5% reflectivity reference surface (in the reference arm).

The reference surface of the interferometer is mounted on a piezoelectric chip (Physik Instrument, PD080.30) which oscillates sinusoidally in the C-scan mode to modulate the interferometric signal at a frequency four times lower than the frequency of the line-scan camera, thus enabling the use of the sinusoidal phase-shifting algorithm described in [26] to extract the

Biomedical Optics EXPRESS

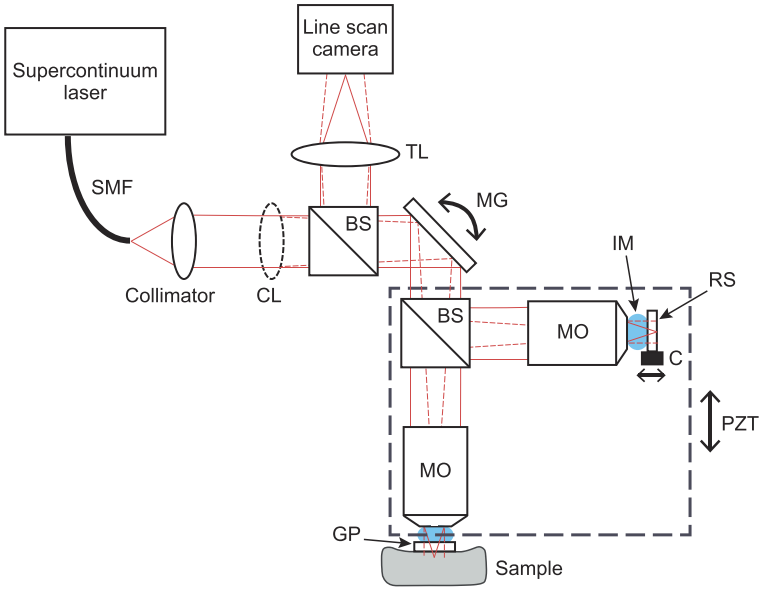

Fig. 1. Schematic of the dual-mode LC-OCT system. SMF: single mode fiber; CL: cylindrical lens; BS: beamsplitter; MG: mirror galvanometer; MO: microscope objective; IM: immersion medium; RS: reference surface; C: piezoelectric chip; PZT: piezoelectric stage; GP: glass plate; TL: tube lens. The plain red lines represent the beam in the plane of the figure (the cylindrical lens has no effect in this plane). The dotted red lines represent the beam in the direction orthogonal to the plane of the figure. The dashed rectangle represents the part of the interferometer moved vertically under the action of PZT for B-scan imaging.

interference fringe envelope. Each line of a C-scan is obtained from an algebraic combination of four consecutive lines acquired by the camera, according to:

$$I = (E_1 - E_2)^2 + (E_3 - E_4)^2. \tag{1}$$

In the B-scan mode, the piezoelectric stage oscillates in a triangular manner at a frequency of 10 Hz, over a travel range of 500 µm in the axial direction, with the camera being used at its maximum frame rate of 70 kHz, resulting in a B-scan of 2048 × 875 pixels (lateral × axial), acquired at a speed of 10 fps [4].

In the C-scan mode, the mirror galvanometer oscillates in a triangular manner at a frequency of 10 Hz over an angular amplitude of 1.6°, resulting in a lateral scan of the sample over 500 µm, with the camera being used at a frame rate of 40 kHz, limited by the maximum frequency of the piezoelectric chip oscillation of 10 kHz, due to both the bandwidth of the amplifier used for the chip (Physik Instrument, E-617) and the mechanical integration of the chip in the reference tank. Considering the frequency of the mirror galvanometer and the frame rate of the camera, 4000 interferometric lines are acquired over the lateral scan, resulting in 1000 intensity lines after application of the phase-shifting algorithm (see Eq. 1). The step between consecutive lines of a C-scan image is of 0.5 µm, which is an appropriate sampling considering an expected lateral resolution of ~ 1 µm. The C-scans are rescaled to 2048 x 875 pixels for proper aspect ratio considering the field of view (FOV) of 1.2 mm × 0.5 mm. As for the B-scans, the C-scans are acquired at a rate of 10 fps.

For both modes, a field-programmable gate array (FPGA, Silicon Software, microEnable V) is used for camera trigging and real-time image acquisition and processing. A custom software written in C++ displays the images obtained from the FPGA board with contrast adjustments

Biomedical Optics EXPRESS

for correct viewing. It is possible to switch from B-scan imaging to C-scan imaging by a click of a button, with a delay of ~ 2 seconds on the screen. It is interesting to note that the B-scans and the C-scans have the same size and acquisition rate, which simplifies the computer process for switching from one mode to the other. When B-scan imaging is performed, the mirror galvanometer can be controlled in order to navigate laterally through the sample. Similarly, when C-scan imaging is performed, the piezoelectric stage can be controlled to navigate in depth through the sample.

3. Results

3.1. Resolution and sensitivity

The imaging axial resolution and detection sensitivity were measured from B-scans, as described in [1]. The axial resolution is 1.2 µm and the sensitivity is 86 dB. Those values were expected since the dual-mode LC-OCT system has not been modified from the original system described in [1] in terms of illumination and detection: identical microscope objectives were used, and the laser power (measured at the output of the optical fiber) was increased from ~ 20 mW to ~ 80 mW to use the camera at the same exposure level.

In order to measure the imaging lateral resolution of the system, a high-resolution microscopy resolution target with line pairs (lp) from 7.5 lp/mm up to 3300 lp/mm was imaged in the C-scan mode. As shown in Fig. 2, the smallest resolvable element has ~ 550 lp/mm, which corresponds to a lateral resolution of ~ 0.9 µm.

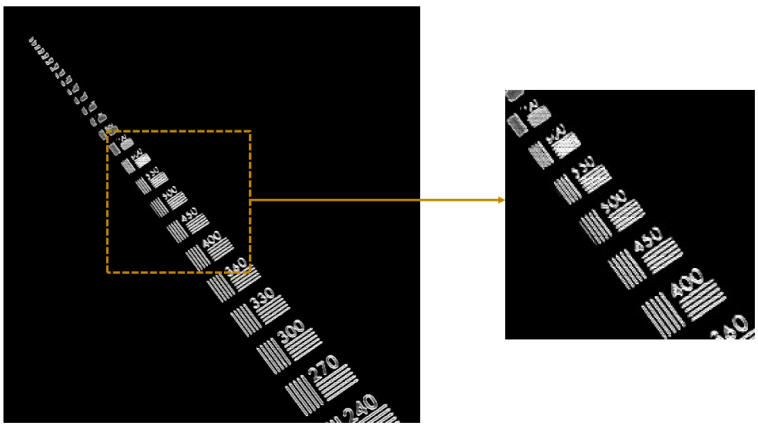

Fig. 2. Lateral resolution characterization for the dual-mode LC-OCT system by C-scan imaging of a high-resolution microscopy resolution target. Line pairs up to 550 lp/mm can be resolved.

3.2. Image acquisition speed

An important characteristic of an imaging system for *in vivo* applications is the acquisition speed. As explained before, the B-scans and C-scans are acquired at 10 fps. This speed may seem low compared to the speeds reported in conventional OCT. However, to properly characterize the speed of an OCT system, the relevant parameter to consider is the amount of extracted information per time [27]. With proper image sampling, this parameter is given, for a 2D image, by the pixel rate

$$P = \frac{N_p}{T}, \tag{2}$$

Biomedical Optics EXPRESS

with N_p the number of pixels in the image and T the duration of the image acquisition. The LC-OCT system reported here generates B-scans and C-scans of 2048 × 875 pixels in 100 ms, resulting in an identical pixel rate for both modes of $P \sim 18$ MPixels/s.

For comparison, the FD-OCT system commercialized by Michelson Diagnostics for skin imaging (VivoSight OCT scanner) has an A-scan rate of 20 kHz and generates B-scans of 1356 × 460 pixels [28]. Therefore its pixel rate for B-scan imaging is ~ 9 MPixels/s, while its pixel rate for C-scan imaging is only ~ 20 kPixels/s (for conventional OCT requiring a 3D image to yield C-scans, the pixel rate for C-scan imaging corresponds to the A-scan rate).

For C-scan imaging though, the comparison is more relevant with OCM systems. FD-OCM systems conventionally require the acquisition of a full 3D volume in order to obtain a C-scan, as in conventional OCT, and therefore suffer from the same speed limitation as FD-OCT. For example, the high speed FD-OCM system proposed in [29] is limited to ~ 560 kPixels/s, ~ 30 times below the pixel rate of our LC-OCT system. Using time-domain point scanning OCM, C-scans can be obtained without the need for acquiring A-scans. Nevertheless, to our knowledge the maximum pixel rate reported with this technique is ~ 4 MPixels/s [30], still below the pixel rate of our LC-OCT system. This highlights the speed advantage of parallelization of the acquisition owing to line-field illumination and detection in a time-domain OCT technique such as LC-OCT. Let us remark that the pixel rate of our LC-OCT system is also much higher than the one of the only other reported line-scanning OCM, of 110 kPixels/s [17]. Nevertheless, it should be noted that a line-field holographic en face OCT system having a resolution approaching that of OCM was recently proposed, with an impressive pixel rate of 205 MPixels/s [31]. By pushing the parallelization forward with FF-OCM, relevant tissue imaging was recently demonstrated at 60 MPixels/s [32] with TD-FF-OCM. Nevertheless, since several interferometric images must be accumulated for skin imaging with FF-OCM, the effective pixel rate of FF-OCM generally does not exceed ~ 3 MPixels/s [20,33]. Let us add that even when the TD-FF-OCM speed approaches that of point or line scan OCM, this implementation is more sensitive to signal losses and artifacts due to sample motion [20,34]. Let us also remark that FD-FF-OCM systems based on swept source lasers have been developed, and although they exhibit very high speed for three-dimensional imaging, they do not have a speed advantage over TD-FF-OCM when C-scan imaging is considered. For example, the state-of-the-art system proposed in [21] has a maximum pixel rate of ~ 20 MPixels/s for C-scan imaging, limited to ~ 650 kPixels/s for relevant skin imaging.

3.3. Application to skin imaging

LC-OCT is a technique that has been shown to have a significant value for skin imaging [4,35]. The dual-mode LC-OCT system reported here has also been specifically developed for skin imaging. The procedure for *in vivo* human skin imaging consists in applying a drop of paraffin oil on the skin and pressing it against the glass plate in the sample arm of the interferometer (see Fig. 1). Paraffin oil provides index matching to suppress the reflection of light at the air/glass interface of the glass plate. The performance of the system is illustrated by imaging healthy skin of the back of the hand of a 25-year-old man. The skin was illuminated with an optical power of ~ 20 mW. Each B-scan or C-scan image consists of an average of 5 images to increase the SNR.

Figure 3 shows four C-scans along with a B-scan obtained by switching from C-scan mode to B-scan mode. The displayed C-scans were obtained at different depths corresponding to different skin layers: stratum corneum, stratum spinosum, stratum basale and papillary dermis. The nuclei of keratinocyte cells are clearly resolved within the epidermis and appear as black spots in the image. Papillae can be identified at the level of the stratum basale. Melanin is identifiable, especially around the papillae. Within the dermis, the structure of collagen networks is also clearly identifiable. The C-scans were obtained with the subject staying still, the depth for imaging being controlled by the piezoelectric stage. The possibility to scan the sample in

Biomedical Optics EXPRESS

depth in real time enables to precisely target and monitor a region of interest. Furthermore, the position of the piezoelectric stage for each C-scan can be looked up within the stroke of the piezoelectric stage for the B-scan, making it possible to exactly correlate the C-scans with the positions to which they correspond in the B-scan, as depicted in Fig. 3. From the B-scan, it is possible to identify to which position of the piezoelectric stage corresponds the surface of the skin and therefore to precisely know at which depth (from the surface of the skin) each C-scan corresponds. The depth for each C-scan in indicated in Fig. 3.

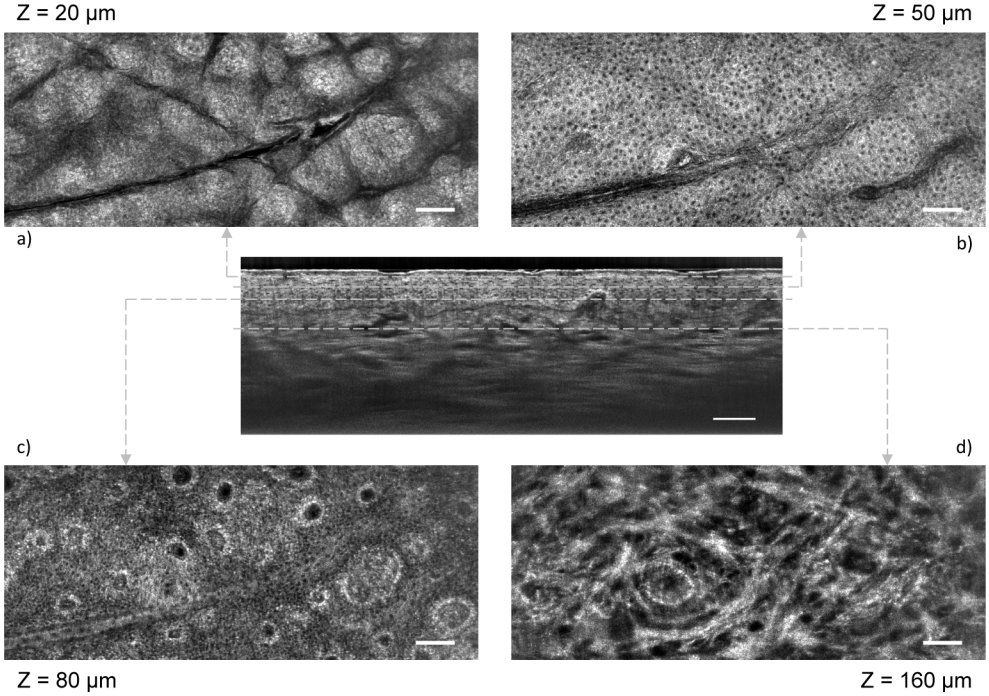

Fig. 3. LC-OCT C-scan images of healthy human skin *in vivo* (back of the hand), obtained for several layers of the skin: a) stratum corneum, b) stratum spinosum, c) stratum basale and d) papillary dermis. The depth (Z) of each layers is indicated, counted from the surface of the skin. The C-scans are correlated to a B-scan obtained by switching from C-scan mode to B-scan mode. Scale bars: 100 µm.

Figure 4 shows four B-scans along with a C-scan. The different lateral positions for imaging in B-scan mode were controlled by scanning the mirror galvanometer. It is therefore possible to navigate laterally in the skin with a resolution of the order of 1 µm, much more accurately and conveniently than scanning the microscope objective or the subject itself as it was previously done in LC-OCT to examine a lesion. The B-scans have a quality similar to the one previously demonstrated for LC-OCT [1]. The epidermis and the dermis can be clearly distinguished. They are separated by the dermal-epidermal junction, where papillae can be identified. The different layers of the epidermis can be identified. The nuclei of keratinocyte cells in the epidermis are resolved. Collagen fibers and blood vessels can be distinguished in the dermis. As it was the case for C-scans, it is possible to correlate exactly the B-scans with the positions to which they correspond in the C-scan by looking up the position of the mirror galvanometer for each B-scan within the stroke of the mirror galvanometer for the C-scan acquisition. The value given in Fig. 4 for the lateral position of the B-scans is counted from the center line of a C-scan. Structures revealed in the en face view in the C-scans are identifiable in cross section in the B-scans. This is particularly clear for structures such as papillae.

Biomedical Optics EXPRESS

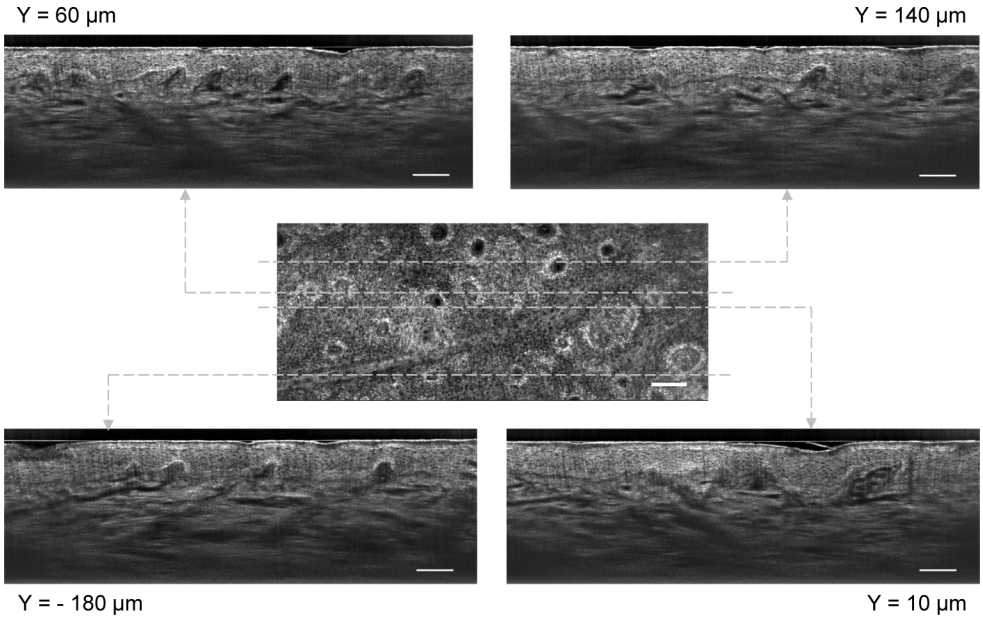

Fig. 4. LC-OCT B-scan images of healthy human skin *in vivo* (back of the hand), obtained for several lateral positions, correlated to a C-scan. The lateral positions (Y) are counted from the center line of the C-scan. Scale bars: 100 µm.

Three-dimensional structures can be identified in both modes, in real time, by switching from one mode to the other at a given position. The fact that the resolution is quasi-isotropic facilitates the analysis and correspondence of the images. Nevertheless, it should be noted that in a realistic clinical context, exact correlation as shown in Figs. 3 and 4 is hardly feasible. The overall acquisition of the eight images took about one minute, mainly due to the time needed to navigate through the skin in the C-scan and B-scan modes to identify interesting regions. Here, the subject was able to remain still for this duration, but it would be more difficult to have no displacement over this duration in a clinical setting, especially when imaging other regions of the body. Nevertheless, the clinical value of this device would not be to exactly correlate the B-scans and C-scans, but rather to have access to both a vertical and a horizontal view of a lesion at cellular resolution, and to be able to navigate through this lesion in both modes, in real time. For an exact correlation of the B-scans and C-scans, three-dimensional imaging would be needed, but the frame rate in the two modes is too low to obtain three-dimensional images over reasonable fields of view in less than ~ 1 minute, which is too long for *in vivo* imaging, especially in a clinical context. LC-OCT thus provides a way to easily analyze three-dimensional structures in real time, at cellular level, without the need for acquisition of true three-dimensional (volumetric) images.

4. Conclusion

We have introduced an extension of the recently proposed LC-OCT technique that combines B-scan and C-scan microscopic imaging. Compared to the original LC-OCT device generating only B-scans, this improved system includes a mirror galvanometer to laterally scan the illumination line, and a high-frequency oscillating piezoelectric chip in the reference arm of the interferometer for modulation of the interferometric signal for C-scan imaging. The resulting system is fairly compact, with the possibility for the user to switch between B-scan and C-scan imaging by a click of a button.

Biomedical Optics EXPRESS

The proposed LC-OCT system can produce B-scans and C-scans with a quasi-isotropic spatial resolution of ~ 1 µm and a detection sensitivity of 86 dB. With a frame rate of 10 fps in both modes, the system can be regarded as a fast OCT/OCM system when the amount of extracted information per time is considered. The horizontal FOV of the C-scans is 1.2×0.5 mm^2, identical to the vertical FOV of the B-scans.

Imaging of human skin *in vivo* at cellular resolution was demonstrated in both B-scan and C-scan modes, with the possibility to navigate within the sample laterally when imaging in the B-scan mode, and in depth when imaging in the C-scan mode. This navigation, coupled to the rapid switch between the acquisition modes, enables to examine precisely and in real time the biological structures of the skin tissues in three dimensions.

This system could provide a valuable alternative to RCM for dermatologists, as it generates horizontal images (C-scans) with a similar lateral resolution, but in addition also provides vertical images (B-scans) having the same microscopic resolution, which is of particular interest for dermatologists as histology also provides vertical images.

Let us also note that the acquisition speed for C-scan imaging could be improved by using a piezoelectric chip with a higher oscillation frequency, in order to eventually be limited by the camera line rate instead of the chip frequency. The acquisition speed could then be improved by using a faster line scan camera. For example, considering the use of a line-scan camera operating at 200 kHz (assuming a laser powerful enough to maintain an acceptable exposure level at this rate) and a chip oscillating at 50 kHz, C-scans could be obtained at a rate of 50 fps. Reaching such a speed could make it possible to consider the acquisition of volumetric images *in vivo*.

Eventually, the compactness of the dual-mode LC-OCT technique makes it possible to consider its integration into a handheld probe, thus providing a powerful tool for dermatologists' daily practice, capable of providing both horizontal images, as in RCM, and vertical images identifiable to histology. This could especially be of major interest in the context of skin cancer screening, where such a tool could help improve the accuracy of clinical diagnostic of skin tumors and reduce the number of surgical excisions of benign lesions.

Disclosures

The authors declare no conflicts of interest related to this article.

References

1. A. Dubois, O. Levecq, H. Azimani, A. Davis, J. Ogien, D. Siret, and A. Barut, "Line-field confocal time-domain optical coherence tomography with dynamic focusing," Opt. Express **26**(26), 33534–33542 (2018).
2. D. Huang, E. A. Swanson, C. P. Lin, J. S. Schuman, W. G. Stinson, W. Chang, M. R. Hee, T. Flotte, K. Gregory, C. A. Puliafito, and J. G. Fujimoto, "Optical coherence tomography," Science **254**(5035), 1178–1181 (1991).
3. A. M. Rollins, M. D. Kulkarni, S. Yazdanfar, R. Ung-arunyawee, and J. A. Izatt, "In vivo video rate optical coherence tomography," Opt. Express **3**(6), 219–229 (1998).
4. A. Dubois, O. Levecq, H. Azimani, D. Siret, A. Barut, M. Suppa, V. del Marmol, J. Malvehy, E. Cinotti, P. Rubegni, and J.-L. Perrot, "Line-field confocal optical coherence tomography for high-resolution noninvasive imaging of skin tumors," J. Biomed. Opt. **23**(10), 1 (2018).
5. W. Drexler, U. Morgner, F. X. Kärtner, C. Pitris, S. A. Boppart, X. D. Li, E. P. Ippen, and J. G. Fujimoto, "In vivo ultrahigh-resolution optical coherence tomography," Opt. Lett. **24**(17), 1221 (1999).
6. G. Humbert, W. J. Wadsworth, S. G. Leon-Saval, J. C. Knight, T. A. Birks, P. S. J. Russell, M. J. Lederer, D. Kopf, K. Wiesauer, E. I. Breuer, and D. Stifter, "Supercontinuum generation system for optical coherence tomography based on tapered photonic crystal fibre," Opt. Express **14**(4), 1596–1603 (2006).
7. Y. Chen, S.-W. Huang, C. Zhou, B. Potsaid, and J. G. Fujimoto, "Improved detection sensitivity of line-scanning optical coherence microscopy," IEEE J. Sel. Top. Quantum Electron. **18**(3), 1094–1099 (2012).
8. A. F. Zuluaga and R. Richards-Kortum, "Spatially resolved spectral interferometry for determination of subsurface structure," Opt. Lett. **24**(8), 519 (1999).
9. B. Grajciar, M. Pircher, A. F. Fercher, and R. A. Leitgeb, "Parallel fourier domain optical coherence tomography for in vivo measurement of the human eye," Opt. Express **13**(4), 1131 (2005).
10. Y. Nakamura, S. Makita, M. Yamanari, M. Itoh, T. Yatagai, and Y. Yasuno, "High-speed three-dimensional human retinal imaging by line-field spectral domain optical coherence tomography," Opt. Express **15**(12), 7103 (2007).

Biomedical Optics EXPRESS

11. S. Lawman, Y. Dong, B. M. Williams, V. Romano, S. Kaye, S. P. Harding, C. Willoughby, Y.-C. Shen, and Y. Zheng, "High resolution corneal and single pulse imaging with line field spectral domain optical coherence tomography," Opt. Express **24**(11), 12395 (2016).
12. M. Mujat, N. V. Iftimia, R. D. Ferguson, and D. X. Hammer, "Swept-source parallel OCT," in *Optical Coherence Tomography and Coherence Domain Optical Methods in Biomedicine XIII*, J. G. Fujimoto, J. A. Izatt, and V. V. Tuchin, eds. (SPIE, 2009).
13. D. J. Fechtig, B. Grajciar, T. Schmoll, C. Blatter, R. M. Werkmeister, W. Drexler, and R. A. Leitgeb, "Line-field parallel swept source MHz OCT for structural and functional retinal imaging," Biomed. Opt. Express **6**(3), 716 (2015).
14. D. J. Fechtig, A. Kumar, W. Drexler, and R. A. Leitgeb, "Full range line-field parallel swept source imaging utilizing digital refocusing," J. Mod. Opt. **62**(21), 1801–1807 (2015).
15. J. A. Izatt, M. R. Hee, G. M. Owen, E. A. Swanson, and J. G. Fujimoto, "Optical coherence microscopy in scattering media," Opt. Lett. **19**(8), 590–592 (1994).
16. A. D. Aguirre, C. Zhou, H.-C. Lee, O. O. Ahsen, and J. G. Fujimoto, "Optical Coherence Microscopy," in *Optical Coherence Tomography - Technology and Applications*, W. Drexler and J. G. Fujimoto, eds. (Springer International Publishing, 2015), p. 865.
17. Y. Chen, S.-W. Huang, A. D. Aguirre, and J. G. Fujimoto, "High-resolution line-scanning optical coherence microscopy," Opt. Lett. **32**(14), 1971 (2007).
18. J. P. Rolland, K. S. Lee, P. Meemon, and S. F. Ibrahim, "Gabor domain optical coherence microscopy of human skin," in *Advances in Dermatological Sciences*, R. Chilcott and K. R. Brain, eds. (Royal Society of Chemistry, 2013), pp. 37–52.
19. C.-C. Tsai, C.-K. Chang, K.-Y. Hsu, T.-S. Ho, M.-Y. Lin, J.-W. Tjiu, and S.-L. Huang, "Full-depth epidermis tomography using a mirau-based full-field optical coherence tomography," Biomed. Opt. Express **5**(9), 3001 (2014).
20. J. Ogien and A. Dubois, "A compact high-speed full-field optical coherence microscope for high-resolution in vivo skin imaging," J. Biophotonics **12**(2), e201800208 (2019).
21. P. Stremplewski, E. Auksorius, P. Wnuk, Ł. Kozoń, P. Garstecki, and M. Wojtkowski, "In vivo volumetric imaging by crosstalk-free full-field OCT," Optica **6**(5), 608–617 (2019).
22. N. Iftimia, G. Peterson, E. W. Chang, G. Maguluri, W. Fox, and M. Rajadhyaksha, "Combined reflectance confocal microscopy-optical coherence tomography for delineation of basal cell carcinoma margins: anex vivostudy," J. Biomed. Opt. **21**(1), 016006 (2016).
23. N. Iftimia, O. Yélamos, C.-S. J. Chen, G. Maguluri, M. A. Cordova, A. Sahu, J. Park, W. Fox, C. Alessi-Fox, and M. Rajadhyaksha, "Handheld optical coherence tomography–reflectance confocal microscopy probe for detection of basal cell carcinoma and delineation of margins," J. Biomed. Opt. **22**(7), 076006 (2017).
24. C. Zhou, D. W. Cohen, Y. Wang, H.-C. Lee, A. E. Mondelblatt, T.-H. Tsai, A. D. Aguirre, J. G. Fujimoto, and J. L. Connolly, "Integrated optical coherence tomography and microscopy for ex vivo multiscale evaluation of human breast tissues," Cancer Res. **70**(24), 10071–10079 (2010).
25. J. Ogien, D. Siret, O. Levecq, H. Azimani, A. David, W. Xue, J. L. Perrot, and A. Dubois, "Line-field confocal optical coherence tomography," in *Optical Coherence Tomography and Coherence Domain Optical Methods in Biomedicine XXIII*, J. A. Izatt and J. G. Fujimoto, eds. (SPIE, 2019).
26. A. Dubois, "A simplified algorithm for digital fringe analysis in two-wave interferometry with sinusoidal phase modulation," Opt. Commun. **391**, 128–134 (2017).
27. W. Wieser, B. R. Biedermann, T. Klein, C. M. Eigenwillig, and R. Huber, "Multi-megahertz OCT: High quality 3d imaging at 20 million a-scans and 45 GVoxels per second," Opt. Express **18**(14), 14685 (2010).
28. D. Zugaj, A. Chenet, L. Petit, J. Vaglio, T. Pascual, C. Piketty, and V. Bourdes, "A novel image processing workflow for the in vivo quantification of skin microvasculature using dynamic optical coherence tomography," Skin Res. Technol. **24**(3), 396–406 (2018).
29. O. O. Ahsen, Y. K. Tao, B. M. Potsaid, Y. Sheikine, J. Jiang, I. Grulkowski, T.-H. Tsai, V. Jayaraman, M. F. Kraus, J. L. Connolly, J. Hornegger, A. Cable, and J. G. Fujimoto, "Swept source optical coherence microscopy using a 1310 nm VCSEL light source," Opt. Express **21**(15), 18021 (2013).
30. M. Pircher, B. Baumann, E. Götzinger, H. Sattmann, and C. K. Hitzenberger, "Phase contrast coherence microscopy based on transverse scanning," Opt. Lett. **34**(12), 1750 (2009).
31. L. Ginner, T. Schmoll, A. Kumar, M. Salas, N. Pricoupenko, L. M. Wurster, and R. A. Leitgeb, "Holographic line field en-face OCT with digital adaptive optics in the retina in vivo," Biomed. Opt. Express **9**(2), 472 (2018).
32. V. Mazlin, P. Xiao, E. Dalimier, K. Grieve, K. Irsch, J.-A. Sahel, M. Fink, and A. C. Boccara, "In vivo high resolution human corneal imaging using full-field optical coherence tomography," Biomed. Opt. Express **9**(2), 557 (2018).
33. M. Boone, G. B. E. Jemec, and V. D. Marmol, "High-definition optical coherence tomography enables visualization of individual cells in healthy skin: comparison to reflectance confocal microscopy," Exp. Dermatol. **21**(10), 740–744 (2012).
34. D. Sacchet, M. Brzezinski, J. Moreau, P. Georges, and A. Dubois, "Motion artifact suppression in full-field optical coherence tomography," Appl. Opt. **49**(9), 1480 (2010).
35. M. Cazalas, O. Levecq, H. Azimani, D. Siret, A. Barut, M. Suppa, V. del Marmol, J. Malvehy, E. Cinotti, P. Rubegni, J. L. Perrot, and A. Dubois, "Skin lesion imaging with line-field confocal optical coherence tomography," in *Photonics in Dermatology and Plastic Surgery 2019*, vol. 10851 B. Choi and H. Zeng, eds., International Society for Optics and Photonics (SPIE, 2019), pp. 61–68.